



Heteroepitaxial integration of freestanding ferroelectric BaTiO₃ on BaZrO₃ membranes

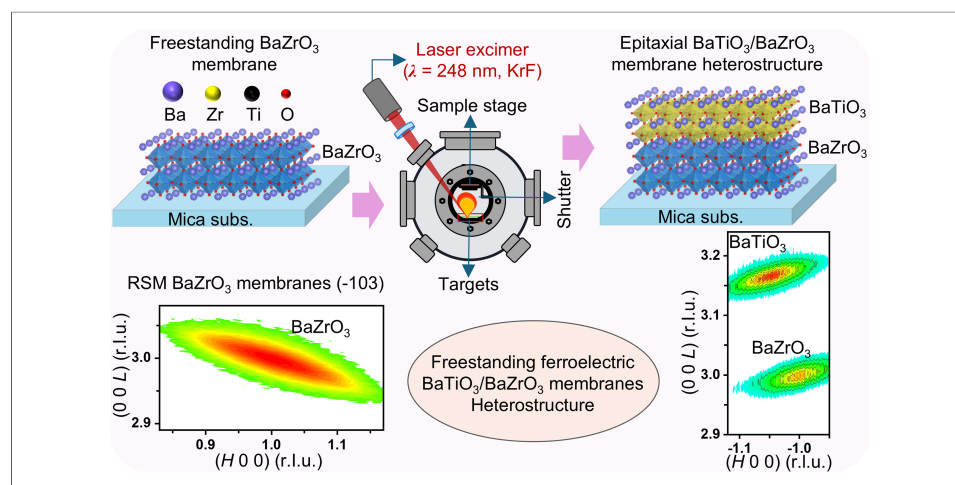
Munir Ahmad¹, Muhammad Sheeraz¹, Seungjae Lim², Jun Won Jang², Ill Won Kim¹, Chang Won Ahn³, Jae-Ung Lee², Jieun Kim⁴, Young-Han Shin¹, Tae Heon Kim^{5,6}

Keywords:

Thin film, oxide, perovskite, freestanding membrane, heteroepitaxy

Citation:

Ahmad, M.; Sheeraz, M.; Lim, S.; Jang, J. W.; Kim, I. W.; Ahn, C. W.; Lee, J. U.; Kim, J.; Shin, Y. H.; Kim, T. H. Heteroepitaxial integration of freestanding ferroelectric BaTiO₃ on BaZrO₃ membranes. *Microstructures* 2026, 6, 2026044. <https://dx.doi.org/10.20517/microstructures.2025.151>



Received: 31 Oct 2025

First Decision: 8 Jan 2026

Revised: 20 Jan 2026

Accepted: 11 Feb 2026

Published: 17 Apr 2026

Academic Editor:

Jungho Ryun

Copy Editor:

Fangling Lan

Production Editor:

Fangling Lan



Abstract

Freestanding oxide membranes, which are free from epitaxial constraint and substrate clamping unlike complex oxide thin-film heterostructures, provide a fascinating platform for realizing multi-functional devices via heterogeneous integration of freestanding membranes with different physical properties. For further applications of freestanding membranes to actual devices, single-crystalline nanomembranes are highly essential. Herein, we demonstrate the fabrication of freestanding BaZrO₃ membranes with high crystallinity via BaZrO₃/SrCuO₂ bilayer thin films epitaxially grown on SrTiO₃ (001) substrates, followed by selective etching of the sacrificial SrCuO₂ layer. The exfoliated freestanding BaZrO₃ membranes serve as a robust template layer for the epitaxial growth of ferroelectric BaTiO₃, producing freestanding BaTiO₃/BaZrO₃ membrane

¹Department of Semiconductor Physics and Engineering, University of Ulsan, Ulsan 44610, Republic of Korea.

²Department of Physics and Department of Energy Systems Research, Ajou University, Suwon 16499, Republic of Korea.

³Basic Science Research Institute and Energy Harvest-Storage Research Center (EHSRC), University of Ulsan, Ulsan 44610, Republic of Korea.

⁴Department of Materials Science & Engineering, Korea Advanced Institute of Science & Technology (KAIST), Daejeon 34141, Republic of Korea.

⁵Electronic and Hybrid Materials Research Center, Korea Institute of Science and Technology (KIST), Seoul 02792, Republic of Korea.

⁶Division of Nanoscience and Technology, KIST School, Korea National University of Science and Technology, Seoul 02792, Republic of Korea.

Correspondence to: Prof. Tae Heon Kim, Electronic and Hybrid Materials Research Center, Korea Institute of Science and Technology (KIST), Seoul 02792, Republic of Korea; Division of Nanoscience and Technology, KIST School, Korea National University of Science and Technology, Seoul 02792, Republic of Korea. E-mail: thkim79@kist.re.kr; Prof. Young-Han Shin, Department of Semiconductor Physics and Engineering, University of Ulsan, Ulsan 44610, Republic of Korea. E-mail: hoponpop@ulsan.ac.kr; Prof. Jieun Kim, Department of Materials Science & Engineering, Korea Advanced Institute of Science & Technology (KAIST), Daejeon 34141, Republic of Korea. E-mail: jkim2024@kaist.ac.kr

heterostructures. The crystallinity and epitaxy of the as-fabricated freestanding heterojunctions is characterized by X-ray diffraction analyses. Raman spectroscopy also reveals that the upper layers of ferroelectric BaTiO₃ are mainly in-plane polarized probably due to the biaxial in-plane tensile strain imposed by the lower BaZrO₃ layer with cubic symmetry, although the initial tensile strain is progressively mitigated with the increasing thickness of the topmost BaTiO₃ layer. The perovskite BaZrO₃ membrane templates are of potential interest for designing strain-tuned heterojunctions of freestanding oxide membranes, where the associated physical properties can be manipulated compared with the bulk counterparts and/or epitaxial oxide thin-film heterostructures.

INTRODUCTION

Perovskite ferroelectric oxides, with their ABO₃ structure, are well-known for their rich electronic, structural, and electromechanical properties that can be precisely controlled in epitaxial thin films and heterostructures^[1–5]. However, conventional rigid substrates impose mechanical constraints^[6] that can diminish intrinsic responses through unavoidable effects such as lattice clamping^[7–9], interfacial constraints^[10], and thermal-mismatch stresses^[11,12]. In recent years, freestanding single-crystal oxide membranes have emerged as an alternative route to decouple functional oxide layers from rigid substrates^[13], enabling large strain gradients^[14,15] and heterogeneous integration with non-oxide substrates (i.e., Si, quartz, metal foil, and polymers) while preserving the crystalline qualities of the exfoliated films^[14,16,17]. These advances of the freestanding membrane heterojunctions have led to a deeper understanding of unusual functional properties and exotic interfacial phenomena which have been uncharted in the typical oxide thin-film epitaxy^[18–20].

Multiple strategies for releasing the topmost film layers from complex oxide thin-film heterostructures and thereafter, for transferring the exfoliated membrane templates on various host substrates have been developed to synthesize freestanding oxide membranes with high crystallinity. A prevailing approach is to utilize a water-soluble Sr₃Al₂O₆ sacrificial layer^[21], enabling heterogeneous integration of freestanding oxide membranes attained by the subsequent epitaxial growth of complex oxides on the as-exfoliated single-crystalline freestanding membranes by lift-off in water^[13,22,23]. Thanks to the pioneering work of freestanding membrane fabrication and heterostructuring via the sacrificial layer, a large variety of chemically etchable sacrificial layers have been found [Supplementary Table 1] and implemented to realize oxide-based freestanding membrane heterojunctions as follows: super-tetragonal non-perovskite Sr₄Al₂O₇ as a high-integrity sacrificial layer^[24], perovskite La_{0.7}Sr_{0.3}MnO₃^[25], YBa₂Cu₃O_{7-x}^[26], BaO^[27], brownmillerite SrCoO_{2.5}^[28], and infinite-layer cuprate SrCuO₂^[23] etched by acid-based solutions in conjunction with complementary “remote epitaxy” techniques employing graphene layers to separate oxide film layers from the underlying substrates^[29,30]. As a direct product of these key achievements in heterogeneously integrating freestanding membranes, it is therefore feasible to manufacture freestanding oxide membrane heterostructures representing monolithic crystallinity and atomically sharp heterointerfaces.

Perovskite BaTiO₃ is of scientific and technological significance among various oxide-based ferroelectric materials due to its remarkable functionalities^[31,32]. Over the last few decades, a wide range of physical properties of bulk BaTiO₃ have been extensively explored^[33,34], attracting enormous interest in the associated fields of oxide electronics^[35,36]. In epitaxial BaTiO₃ thin films, both ferroelectric and dielectric properties of the strained BaTiO₃ films are greatly enhanced compared to the bulk counterparts owing to misfit strain arising from a lattice mismatch between the films and the underlying substrates^[31,32,36,37]. For instance, the ferroelectric-to-paraelectric transitions of in-plane compressively strained BaTiO₃ films occur at several hundred degrees higher temperatures than the bulk compounds^[38]. It is intriguing that freestanding BaTiO₃ membranes are super-elastic and ultra-flexible leading to reversible domain reconfiguration by mechanical

bending, giant electromechanical responses, and dynamic strain-engineered polarization states that are unattainable in substrate-clamped films^[39,40]. It has been also reported that continuous dipole rotation in super-elastic BaTiO₃ membranes is accessible via reversible mechanical bending in addition to sizable piezoelectric and/or flexoelectric couplings^[40]. However, systematic studies on bi-axially tensile-strained freestanding BaTiO₃ membranes have been rare for in-depth understanding of microscopic polarization states and domain configurations.

For this aim, we choose oxide perovskite BaZrO₃ as a base template layer for the secondary epitaxial growth of ferroelectric BaTiO₃^[31,41,42]. Ternary BaZrO₃ has been identified as an effective template for strain regulation in BaTiO₃. Recently, it has been demonstrated that cubic BaZrO₃ substrates impose strong square-tensile-strain on BaTiO₃, stabilize in-plane polarization states, and enable reversible control of ferroelectric and dielectric responses through strain engineering^[31]. In addition to its strain-engineering capability, the band-insulating BaZrO₃ is an excellent platform for heterogeneously integrating with ferroelectric materials and for fabricating thin-film based electronic devices due to its high dielectric permittivity and low dielectric loss^[41–43]. In a structural point of view, the BaZrO₃ has a cubic symmetry ($Pm\bar{3}m$) with a large lattice parameter (4.189 Å), which allows us to apply high biaxial strain to realize in-plane polarized ferroelectric thin films^[31]. Importantly, in a freestanding heterojunction geometry, the BaZrO₃ membrane template layer can act as a substrate, which is commercially not available, enabling strain tuning in epitaxial membrane heterostructures with reduction of a mechanical clamping effect arising from conventional rigid substrates. This is our motivation of epitaxial synthesis of highly crystalline freestanding oxide membrane heterojunctions. Once an oxide membrane is released, it can elastically redistribute surface morphology/curvature to accommodate strain alleviation and thus, mechanical states unavailable in substrate-bonded heterostructures are accessible^[44]. Thanks to these advantages, freestanding BaZrO₃ membranes with high crystallinity are a prerequisite for synthesizing freestanding ferroelectric heterojunctions under large in-plane tensile strain. The as-fabricated freestanding ferroelectric BaTiO₃/BaZrO₃ heterojunctions transferred on non-perovskite host substrates should be highly elastic and flexible, because they are free from substrate clamping effects^[23].

In this work, we report the heteroepitaxial integration of ferroelectric BaTiO₃ films on freestanding BaZrO₃ membranes. A facile route is established to fabricate highly crystalline freestanding BaZrO₃ membranes using chemically etchable SrCuO₂ sacrificial layers on top of BaZrO₃/SrCuO₂ on SrTiO₃ (001) substrates^[23]. Furthermore, we demonstrate the heteroepitaxial growth of ferroelectric BaTiO₃ on BaZrO₃ membrane templates through comprehensive characterization including X-ray diffraction (XRD), reciprocal space mappings (RSMs), atomic force microscopy (AFM), and ultraviolet (UV)-Raman spectroscopy. The combination of ferroelectric BaTiO₃ with freestanding BaZrO₃ membranes in substrate-decoupled architectures provides an opportunity for dynamic strain and flexoelectric engineering of ferroelectric heterojunctions transferred on non-oxide substrates.

MATERIALS AND METHODS

Synthesis of BaZrO₃, SrCuO₂, and BaTiO₃ pulsed laser deposition (PLD) targets

Cubic perovskite BaZrO₃ powders were synthesized using a conventional solid-state reaction method. Barium carbonate (BaCO₃ ≥ 99.99%, Sigma-Aldrich, St. Louis, Missouri, USA) and zirconium dioxide (ZrO₂ ≥ 99.99%, US Research Nanomaterials, Houston, Texas, USA) were used as starting materials. Both powders were placed in the beaker and initially dried for 24 h in an electric oven. Then, stoichiometric amounts of high-purity, dried BaCO₃ and ZrO₂ powders were weighed to achieve a nominal Ba:Zr molar ratio of 1:1. The precursor powders were placed in a bottle with Zr balls and ethanol (1:1:3), and ball-milled for 24 h at 200 rev/min. After drying process, the powders were dissolved for 24 h and thoroughly ground in an agate

mortar and pestle for 30–60 min to ensure compositional homogeneity. Repeat these steps two times. After mixing thoroughly, the powder mixture was calcined in air at 1,300 °C for 2 h in the box furnace (see [Supplementary Figure 1](#)) to decompose residual BaCO₃ and promote the formation of the single-phase perovskite BaZrO₃. The calcined powders were subsequently reground and sieved to eliminate hard agglomerates and ensure phase purity. For PLD target fabrication, 15 g of the calcined BaZrO₃ powder was blended with a polyvinyl alcohol (PVA) binder solution, loaded into a 1-inch diameter mold, and uniaxially pressed under 5 tons of hydraulic load for 30 s (see [Supplementary Figure 1](#)). The target was then sintered at 1,650 °C for 4 h, followed by surface polishing to obtain a dense and smooth BaZrO₃ target suitable for PLD deposition. Similarly, SrCuO₂ and BaTiO₃ 1-inch PLD targets were synthesized using the aforementioned steps for thin-film fabrication (see [Supplementary Figure 1](#)). The calcination and sintering conditions for the SrCuO₂ PLD target (1-inch) in the box furnace were 600 °C for 4 h and 900 °C for 24 h, respectively, in air for chemical reaction. However, for the BaTiO₃ target, the calcination and sintering conditions in the box furnace were 1,100 °C for 8 h and 1,330 °C for 6 h, respectively, in air for chemical reaction^[45].

Fabrication of epitaxial BaZrO₃/SrCuO₂ bilayer thin films

BaZrO₃/SrCuO₂ bilayer thin films were fabricated on single-crystal SrTiO₃ (001) substrates (< 0.1°, 10 mm × 10 mm × 0.5 mm, CrysTec, Köpenicker, Berlin, Germany) by PLD (DADA Korea Co., Ltd., South Korea). Growth began with the deposition of an SrCuO₂ sacrificial layer [[Supplementary Table 1](#)], followed by the subsequent deposition of the BaZrO₃ top layer. All depositions were carried out in a vacuum chamber with a base pressure of 1.1×10^{-7} Torr, equipped with ceramic SrCuO₂ and BaZrO₃ targets, and SrTiO₃ (001) substrates were mounted on a heated stage. The substrate heater was stabilized at 617 °C, and the oxygen partial pressure was adjusted to 50 mTorr. A KrF excimer laser ($\lambda = 248$ nm, COMPex 201F, COHERENT Laser System, GmbH & Co. KG, Hans-Böckler-Straße 12, 37079 Gottingen, Germany) operating at 5 Hz with a laser energy density of 1.2 J cm⁻² and a laser spot area of 7 mm² was used for ablation. Prior to film deposition, the SrCuO₂ and BaZrO₃ targets were pre-ablated for 10 min to remove surface contaminants. Under these conditions, epitaxial SrCuO₂ thin films with the average thickness of ~40 nm were deposited on SrTiO₃ (001) substrates. Subsequently, the BaZrO₃ target was rotated into the laser path, and the BaZrO₃ layer (~30 nm) was grown under identical conditions. After deposition, the samples were cooled down to room temperature with a ramping rate of 10 °C min⁻¹ under atmospheric oxygen pressure (~760 Torr).

Fabrication of freestanding BaZrO₃ membranes

Freestanding BaZrO₃ membranes were synthesized by selectively etching the SrCuO₂ sacrificial layers (for more details of etching conditions, see [Supplementary Table 1](#)) from the as-grown BaZrO₃/SrCuO₂ bilayer films on SrTiO₃ (001) substrates. The samples were immersed in an aqueous etching solution composed of 8 mg KI, 10 mL HCl, and 100 mL H₂O^[23]. During etching, the SrCuO₂ layers completely dissolved, releasing the floating BaZrO₃ membranes on the water surface. To transfer the as-exfoliated membranes onto host substrates (e.g., mica, Pt/Si, and Si), the SrTiO₃ substrates were extracted from the solution, and the desired host substrates were gently inserted using tweezers. The floating BaZrO₃ membranes were then transferred onto the host substrates, yielding highly crystalline freestanding BaZrO₃ membranes with little structural disorder (e.g., cracks, wrinkles, and bending). The transferred membranes were subsequently lifted out of the beakers using tweezers.

Heteroepitaxial integration of ferroelectric BaTiO₃ on freestanding BaZrO₃ membranes

Ferroelectric BaTiO₃ thin films were epitaxially grown on freestanding BaZrO₃ membranes supported on bare and Au-coated mica substrates (9.9 mm Highest grid mica disc, MTI Corporation, Richmond, CA 94804, USA) by PLD. The substrate heater was set to 707 °C, and the oxygen partial pressure, laser repetition rate, and laser fluence were adjusted to 25 mTorr, 5 Hz, and 1.2 J cm⁻², respectively. The BaTiO₃ target was pre-ablated for 10 min before film deposition. BaTiO₃ thin films with thicknesses of ~10, 25, 50, 100, and

140 nm were grown under identical conditions. Then, the samples were *in situ* annealed at 707 °C for 30 min under an oxygen partial pressure of 25 mTorr and cooled down to room temperature with a ramping rate of 10 °C min⁻¹.

X-ray diffraction (XRD) analyses

Structural characterization was performed using both laboratory and synchrotron XRD. θ -2 θ scans of single-layer BaZrO₃, SrCuO₂, and BaTiO₃ films in addition to bilayer BaZrO₃/SrCuO₂ heterostructures on SrTiO₃ (001) and BaTiO₃ films grown on freestanding BaZrO₃ membranes/mica were collected with a four-circle X-ray diffractometer (Cu K α 1 radiation, λ = 1.5406 Å; monochromated; D8 Advance, Bruker, Germany). High-resolution synchrotron XRD was performed at the 3A beamline of the Pohang Accelerator Laboratory (PAL), POSTECH, using a six-circle diffractometer. RSMs were employed to evaluate the lattice parameters and to identify the in-plane lattice coherency. For BaZrO₃, SrCuO₂ single-layer, and BaZrO₃/SrCuO₂ bilayer films on SrTiO₃ (001) substrates, RSMs around the (-103) Bragg diffractions of the SrTiO₃ (001) substrates were performed using the laboratory diffractometers. The in-plane and out-of-plane lattice parameters were extracted from *H*- and *L*-scans. High-resolution RSMs of the as-transferred freestanding BaZrO₃ membranes were obtained at PAL, and the corresponding lattice parameters derived from the obtained (-103) RSMs of the freestanding BaZrO₃ membranes. Rocking-curve analyses were used to evaluate film crystallinity. Full-width at half maximum (FWHM) values of the thickness-dependent BaTiO₃ films on freestanding BaZrO₃ membranes/mica were determined from the Lorentzian fits of the (002) rocking curves. Similar measurements were performed for freestanding BaZrO₃ membranes and freestanding ferroelectric BaTiO₃/BaZrO₃ heterojunctions using synchrotron XRD. The film thicknesses of BaZrO₃, SrCuO₂, and BaTiO₃ single-layer films grown on SrTiO₃ (001) substrates were evaluated by X-ray reflectivity (XRR). The observed thickness oscillations (i.e., Kiessig fringes) were fit using the LEPTOS software (Bruker, Germany).

Atomic force microscopy (AFM) measurements

Surface morphology was examined using AFM (Nanocute with Nanonavi-II Station, Nano Fine Tech, Japan) in ambient conditions. Measurements were performed on single-layer BaZrO₃, SrCuO₂, and BaTiO₃ films, BaZrO₃/SrCuO₂ bilayer films on SrTiO₃ (001) substrates and freestanding BaZrO₃ membranes transferred onto mica and Pt/Si substrates. The dynamic force microscopy (DFM) tips with a spring constant of ~42 N m⁻¹ and a tip radius < 10 nm were used at a resonance frequency of ~320 kHz.

Raman spectroscopy measurements

A continuous-wave He-Cd laser (325.0 nm, Kimmon Koha, Japan) was employed as the excitation source. The laser beam was focused onto the sample through a 50 × UV-enhanced objective lens (Mitutoyo, Japan), which was also used to collect the backscattered signal. The Raman-scattered light was dispersed by a spectrometer (IsoPlane 320, Princeton Instruments, USA) equipped with a 2,400 grooves mm⁻¹ grating and subsequently detected with a back-illuminated charge-coupled device (PIXIS 400BRX, Princeton Instruments, USA).

RESULTS AND DISCUSSION

To investigate the feasibility of fabrication of freestanding ferroelectric BaTiO₃/BaZrO₃ membrane heterostructures, we first optimized the growth conditions of BaZrO₃ [Supplementary Figure 2], SrCuO₂ single-layer films [Supplementary Figure 3], and BaZrO₃/SrCuO₂ bilayer films on SrTiO₃ (001) substrates [Figure 1]. The detailed growth conditions of single-layer and bilayer films are presented in the Materials and Methods section and Supplementary Materials. To synthesize the freestanding BaZrO₃ membranes, we first

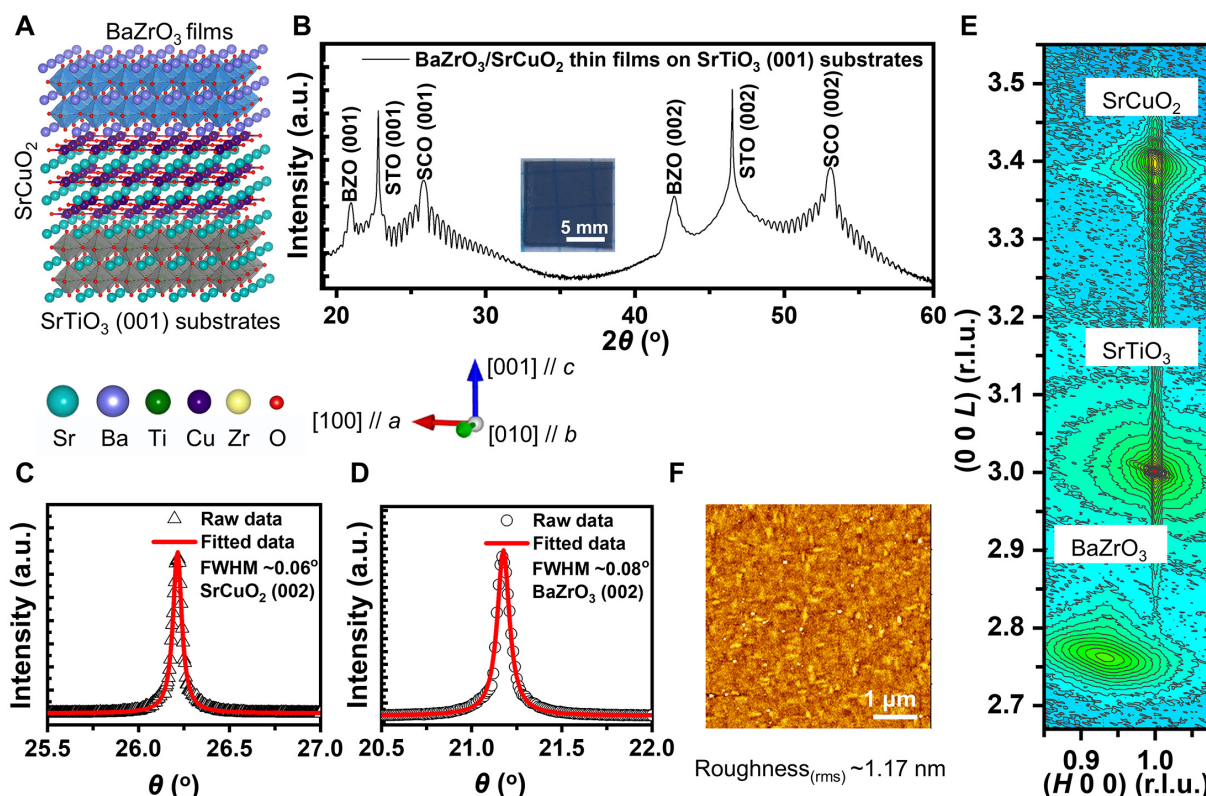


Figure 1. Synthesis and characterization of BaZrO₃ (~30 nm)/SrCuO₂ (~40 nm) bilayer thin films grown on SrTiO₃ (001) substrates. (A) Schematic of epitaxial growth of BaZrO₃/SrCuO₂ bilayer thin films on SrTiO₃ (001) substrates. (B) Synchrotron XRD θ -2 θ scan of BaZrO₃/SrCuO₂ bilayer thin films, and optical image of bilayer sample (inset). (C and D) Rocking-curve measurements of the BaZrO₃ (002) and SrCuO₂ (002) peaks with the FWHM values of ~0.08° and ~0.06°, respectively. (E) RSMs of BaZrO₃/SrCuO₂ bilayer thin films around the (-103) Bragg peaks of SrTiO₃ (001) substrates. (F) The AFM topography images of epitaxial BaZrO₃/SrCuO₂ bilayer thin films grown on SrTiO₃ (001) substrates with surface roughness (rms) of ~1.17 nm.

prepared epitaxial BaZrO₃ (~30 nm)/SrCuO₂ (~40 nm) bilayer films on top of the SrTiO₃ (001) substrates as depicted in Figure 1A. The XRD results showed that the as-grown BaZrO₃/SrCuO₂ bilayer thin films were highly crystalline and epitaxial [Figure 1B]. The thickness of each layer was determined using XRR (see Supplementary Figures 2 and 3). The rocking-curve measurements of the (002) SrCuO₂ Bragg peaks in the BaZrO₃/SrCuO₂/SrTiO₃ (001) heterostructures evidenced high crystalline quality with the FWHM value of ~0.06° as depicted in Figure 1C, which was almost close to that of single-layer SrCuO₂ (~0.05°) (see Supplementary Figure 3 and Supplementary Table 2). However, the FWHM value (~0.08°) of the upper BaZrO₃ layer was obtained from the rocking-curve result of the BaZrO₃ (002) Bragg peak in the bilayer BaZrO₃/SrCuO₂ film (see Figure 1D and Supplementary Table 2), which was twice larger than that (FWHM ~0.04°) of the single-layer BaZrO₃ thin film on SrTiO₃ in (see the inset of Supplementary Figure 2). Along with the rocking-curve measurements of the BaZrO₃/SrCuO₂/SrTiO₃ (001) heterostructures, the RSMs showed that the SrCuO₂ layers were coherent with respect to the SrTiO₃ substrates, while the BaZrO₃ layers were partially relaxed [Figure 1E]. The extracted lattice parameters of both the SrCuO₂ and BaZrO₃ layers were summarized in Supplementary Table 3. The AFM topography images of the BaZrO₃/SrCuO₂ films exhibited higher surface roughness of ~1.17 nm [Figure 1F] compared with single-layer BaZrO₃ (~0.23 nm) and SrCuO₂ (~0.23 nm) films on SrTiO₃ substrates [Supplementary Figures 2 and 3].

To prepare freestanding BaZrO₃ membranes, we first dissolved the sacrificial SrCuO₂ (~40 nm) layer via chemical etching in a diluted KI etchant solution^[23]. Next, the as-released freestanding BaZrO₃ membranes were transferred to various non-perovskite host substrates (i.e., mica, Pt/Si, and Si) using the lift-off

technique, as described in Figure 2A. The high-resolution XRD results showed that the crystallographic direction was mainly (001)-oriented with no secondary phase [Figure 2B and Supplementary Figure 4], indicating that the epitaxy of the as-transferred freestanding BaZrO₃ membranes remained. The rocking curves of the (002) Bragg peak of freestanding BaZrO₃ membranes revealed a FWHM value of $\sim 0.31^\circ$ [Figure 2C]. The relatively poor crystallinity of the freestanding BaZrO₃ membranes would be attributed to the further relaxation^[31] of the initial in-plane compressive strain, formation of the local disorder (i.e., cracks, wrinkles, and bending) during chemical etching and the following transfer process of the freestanding membranes, as shown in photographic image [Figure 2D]^[23]. For more details and lateral dimensions of the resultant freestanding BaZrO₃ membranes transferred to various host substrates, see Supplementary Figure 5. The AFM topographic images revealed that the surface roughness of the freestanding BaZrO₃ membranes increased to ~ 3.12 nm [Figure 2E], almost three times larger than the root-mean-square (rms) values of ~ 1.17 nm obtained for the BaZrO₃/SrCuO₂ bilayer films [Figure 1F]. Using the synchrotron RSM measurement around the (-103) Bragg peaks of the freestanding BaZrO₃ membranes [Figure 2F], we estimated the lattice parameters of the as-fabricated freestanding BaZrO₃ membranes [Supplementary Table 3]. After the alleviation of the huge misfit strain, the crystalline quality of our freestanding BaZrO₃ membranes was comparable to those of other freestanding membranes and epitaxial thin films and thus, they could be utilized as a template layer for the epitaxial thin-film growth of ferroelectric BaTiO₃.

Prior to the synthesis of the freestanding ferroelectric BaTiO₃/BaZrO₃ heterojunctions, we first optimized PLD growth conditions of BaTiO₃ single-layer films on SrTiO₃ (001) substrates [Supplementary Figure 6]. Herein, the epitaxy and crystallinity of the as-grown BaTiO₃ films were confirmed with the XRD θ -2 θ scans and rocking curves of epitaxial BaTiO₃ thin films, respectively. It appeared that the surface roughness of the BaTiO₃ thin films was ~ 3.62 nm and the corresponding thickness was calibrated to ~ 25 nm through the XRR analyses.

To manufacture epitaxial freestanding ferroelectric BaTiO₃/BaZrO₃ membrane heterostructures further, we mounted the as-fabricated freestanding BaZrO₃ membranes on mica in a vacuum chamber and directly deposited ferroelectric BaTiO₃ (~ 25 nm) layers on top of the freestanding BaZrO₃ membranes (~ 30 nm)/mica [Figure 3A]. Note that we also transferred the freestanding BaZrO₃ membranes on other host substrates such as Si and Pt/Si. Subsequently, the structural integrity of the as-deposited freestanding ferroelectric BaTiO₃/BaZrO₃ membrane heterostructures was confirmed by XRD analyses. The θ -2 θ scans in Figure 3B showed the diffraction patterns exhibiting the (00 l) Bragg peaks of BaZrO₃ and (h 00)/(00 l) Bragg peaks of BaTiO₃ in addition to (00 l) Bragg peaks of mica substrates. The inset photograph in Figure 3B also displayed the successful fabrication of BaTiO₃/BaZrO₃ membrane heterostructures with a millimeter scale of lateral dimensions.

To evaluate the epitaxial quality, rocking-curve measurements were performed on the (002) Bragg peak of BaZrO₃ [Figure 3C] and the (200) Bragg peak of BaTiO₃ [Figure 3D]. The FWHM value of $\sim 0.37^\circ$ for the (200) Bragg peak of BaTiO₃ indicated the relatively poor crystallinity of the BaTiO₃ layer compared to the BaZrO₃ layer ($\sim 0.30^\circ$) [Supplementary Table 2]. From the θ -2 θ scans, the out-of-plane lattice parameter of BaZrO₃ was found to be ~ 4.211 Å, which was close to bulk cubic BaZrO₃ ($c = 4.189$ Å)^[31] [Supplementary Table 3]. It was highly likely that the freestanding BaZrO₃ membranes were fully relaxed. In contrast, the out-of-plane lattice parameter of BaTiO₃ was estimated to be ~ 4.014 Å, which was less than the c lattice constant ($c = 4.038$ Å) of bulk tetragonal BaTiO₃ and rather, analogous to the a/b lattice constant ($a = b$

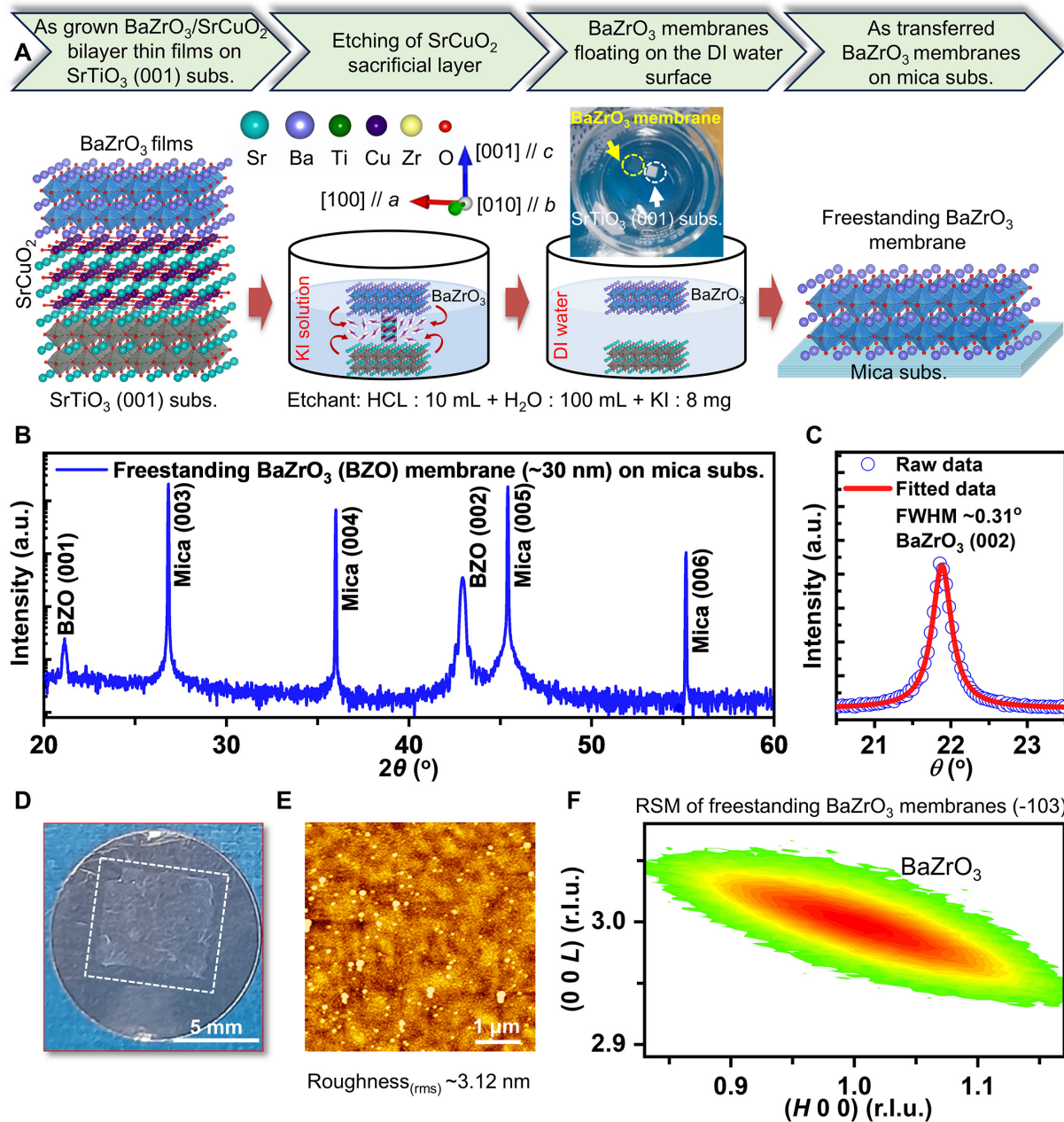


Figure 2. Synthesis and characterization of freestanding BaZrO_3 (~30 nm) membranes. (A) Schematic figures of the fabrication of BaZrO_3 membranes via etching of SrCuO_2 sacrificial layers using KI solutions [HCl: 10 mL + H_2O : 100 mL + KI: 8 mg]. (B and C) The XRD analyses of the as-transferred ($5 \times 5 \text{ mm}^2$) single-crystalline freestanding BaZrO_3 membranes on mica substrates and the corresponding rocking-curve data of the (002) BaZrO_3 Bragg peaks. (D) Photographs of the as-transferred freestanding BaZrO_3 membranes on mica substrates. (E) The AFM topography images of the as-transferred freestanding BaZrO_3 membranes. (F) The RSMs data for verifying the BaZrO_3 peaks positions around the (-103) Bragg peaks of the freestanding BaZrO_3 membranes.

$= 3.992 \text{ \AA}$)^[23,31] [Supplementary Table 3]. This indicated that the lower freestanding BaZrO_3 membranes imposed in-plane tensile strain on the upper BaTiO_3 films. Note that the in-plane lattice mismatch between bulk BaTiO_3 ($a = 3.992 \text{ \AA}$) and bulk BaZrO_3 ($a = 4.189 \text{ \AA}$) was $\sim 4.9\%$ ^[31]. Therefore, huge biaxial tensile strain should be loaded on BaTiO_3 in the freestanding ferroelectric $\text{BaTiO}_3/\text{BaZrO}_3$ membrane heterostructures. Herein, the roughness of the as-grown BaTiO_3 surfaces was approximately 9.62 nm [Figure 3E]. Intriguingly,

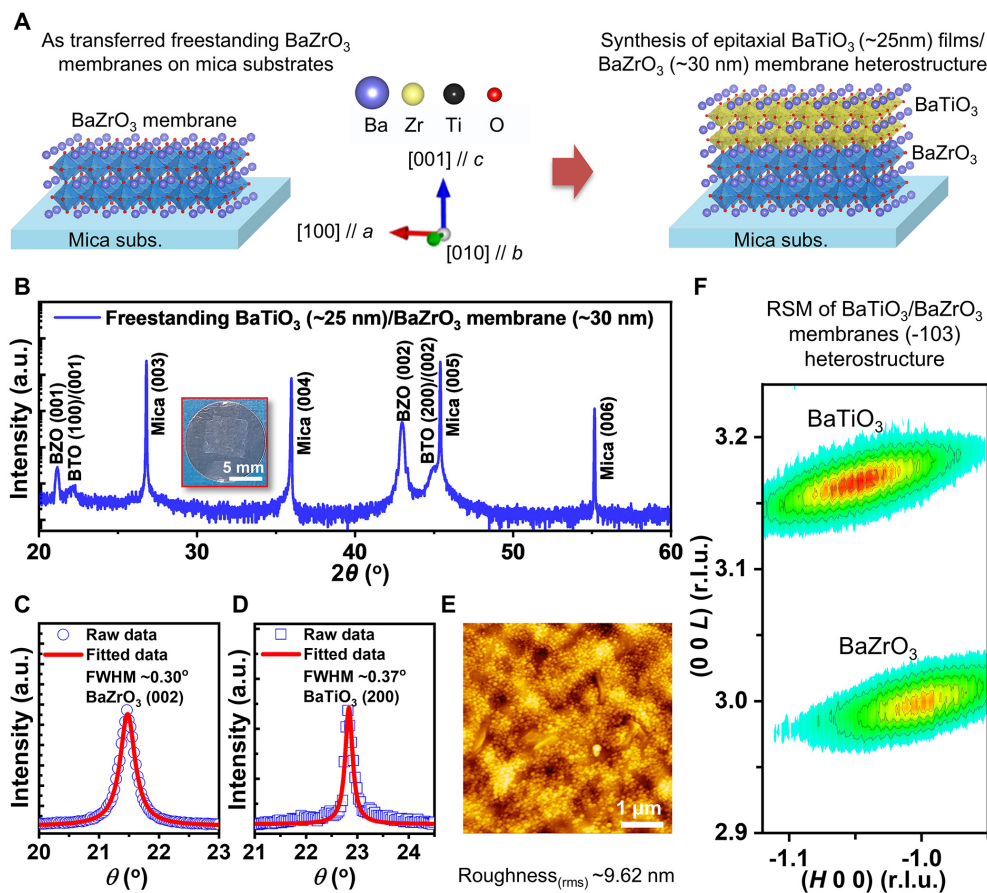


Figure 3. Synthesis and characterization of freestanding ferroelectric BaTiO₃ (~25 nm)/BaZrO₃ (~30 nm) membrane heterostructures. (A) Schematic figures of the as-transferred freestanding BaZrO₃ membrane (5 × 5 mm²) and the following thin-film growth of ferroelectric BaTiO₃ for manufacturing freestanding ferroelectric BaTiO₃/BaZrO₃ membrane heterojunctions on mica substrates. (B) The XRD analyses of the as-grown freestanding ferroelectric BaTiO₃/BaZrO₃ membrane heterostructures on mica substrates. The inset indicates photographs of the as-fabricated BaTiO₃/BaZrO₃ membrane heterojunctions. (C and D) Rocking-curve results of the BaZrO₃ (002) and BaTiO₃ (200) peaks in freestanding BaTiO₃/BaZrO₃ bilayer membranes. (E) The AFM topography images of the as-grown freestanding ferroelectric BaTiO₃/BaZrO₃ membrane heterostructures. (F) RSMs of freestanding BaZrO₃/BaTiO₃ bilayer membranes around the (-103) Bragg peaks of the freestanding BaZrO₃ membranes.

emergence of the mixed domain states of ($c + a$) was observed in the BaTiO₃ films, as evidenced by the coexistence of the (002) and (200) diffraction peaks (see also [Supplementary Figures 6 and 7](#)). To further estimate the lattice parameters of the BaTiO₃ layers with the mixed domain structures, we carried out the RSM measurements (see [Figure 3F](#)) of the freestanding BaTiO₃/BaZrO₃ membrane heterojunctions around the (-103) Bragg peaks of the underlying BaZrO₃ membrane templates. It was evident that the initial biaxial tensile strain in the BaTiO₃/BaZrO₃ bilayer membranes was relaxed with formation of the mixed domain configurations of tetragonal ($c + a$). The estimated lattice parameters of the BaTiO₃ and BaZrO₃ in the freestanding BaTiO₃/BaZrO₃ membrane heterojunction were summarized in [Supplementary Table 3](#).

To investigate effects of film thickness on strain states and the associated domain configurations, we progressively changed the BaTiO₃ film thickness from ~10 to ~140 nm while keeping the BaZrO₃ membrane thickness constant (~30 nm), as shown in [Figure 4A](#). The θ -2 θ scans [[Figure 4A](#)] showed that all BaTiO₃/BaZrO₃ bilayer membranes with different thickness exhibited both (00 l) peaks of BaZrO₃ and (00 l)/(h 00) peaks of BaTiO₃ implying that the bilayer membrane samples were almost epitaxial with no impurity phase. In rocking-curve results of the (200) Bragg peaks of the upper BaTiO₃ layer [[Figure 4B](#)], we identified that the measured FWHM values varied with non-monotonic characteristics in the range of 0.02 to

0.41°. At the ultrathin limit of ~10 nm, the FWHM was as narrow as ~0.09°, indicative of high crystallinity of our BaTiO₃/BaZrO₃ bilayer thin-film membranes with little texturing. As the thickness increased, the FWHM increased (up to ~0.41° for 50-nm-thick BaTiO₃/BaZrO₃ bilayer membranes), probably due to thickness-induced strain relaxation and the linked defect formation. Remarkably, for thick BaTiO₃/BaZrO₃ bilayer membranes above ~100 nm, the FWHM became narrow again (~0.09° for 140-nm-thick bilayer membranes). Meanwhile, the (002) Bragg peaks of the lower BaZrO₃ (~30 nm) membranes exhibited relatively large FWHM values (0.68°–1.14°) compared with the upper BaTiO₃ films. This indicated that the thinner BaZrO₃ membranes were more textured with the incorporating defects than the upper BaTiO₃ film layer and nevertheless, the crystalline quality of the freestanding BaZrO₃ membranes were good enough to hetero-epitaxially integrate the ferroelectric overlayers, serving as effective templates to manufacture single-crystalline freestanding ferroelectric heterojunctions.

Figure 4C represented the lattice parameters of freestanding BaZrO₃ membranes and the as-integrated BaTiO₃/BaZrO₃ membrane heterostructures as a function of the BaTiO₃ thickness, respectively. Regardless of the thickness, the freestanding BaZrO₃ membranes (marked by blue solid circles) exhibited lattice parameters corresponding to the bulk cubic value (~4.189 Å), indicating that the as-released freestanding BaZrO₃ membranes were fully relaxed close to cubic BaZrO₃. This highlighted the advantage of the freestanding geometry, in which there was no substrate clamping and epitaxial constraint imposed by the underlying substrate and thereby, the cubic BaZrO₃ membrane templates were suitable for the secondary film growth of ferroelectric BaTiO₃. In the BaTiO₃ films grown on freestanding BaZrO₃ membranes, a clear tetragonal distortion was observed with concurrent tetragonal *c* (marked by orange solid triangles) and *a* (marked by green solid squares) lattice constants (for more details, see [Supplementary Figure 7](#) and [Supplementary Table 3](#)), in agreement with those of bulk BaTiO₃ (*c* = ~4.038 Å, *a* = ~3.992 Å)^[23,31]. It was also worthwhile to note that a single state of tetragonal *a* domain was predominant for the ultrathin 10-nm-thick BaTiO₃/BaZrO₃ membrane heterojunctions due to the biaxial tensile strain imposed by cubic BaZrO₃, whereas the in-plane tensile strain began to mitigated with the increasing BaTiO₃ thickness (above ~25 nm) leading to emergence of a mixed domain configuration of tetragonal (*c* + *a*).

As depicted in a plot of FWHM versus BaTiO₃ film thickness [Figure 4D], the BaTiO₃ film layers for all BaTiO₃/BaZrO₃ bilayer membranes exhibited sharper spectral shapes of the (200) diffraction peaks (denoted by orange open squares) compared with the (002) diffraction peaks (denoted by blue open circles) of underlying BaZrO₃ membrane templates. Such enhancement of the crystallinity of the upper BaTiO₃ layers, that was phenomenologically named epitaxial “self-healing” [Supplementary Figure 8A–C], would be attributed to strain redistribution and the resulting reduction of structural defects during the secondary thin-film growth of ferroelectric BaTiO₃ overlayers via pulsed laser epitaxy. Particularly, the “self-healing” characteristics were likely to be applicable for realizing freestanding oxide membrane heterojunctions representing better crystallinity like oxide single crystals. It should be also noted that the as-integrated freestanding ferroelectric BaTiO₃/BaZrO₃ heterojunctions were scalable in the wide range of film thickness in conjunction with retention of high crystallinity. The “self-healing” behaviors were reminiscent of previous studies^[46] on other freestanding perovskite oxides such as SrTiO₃ and PbTiO₃ membranes, where gradual strain relaxation and enhanced electromechanical responses have been reported^[43,47–49]. Notably, Elangovan *et al.* demonstrated that freestanding perovskite oxide membranes retained both crystallinity and flexibility even under large mechanical stress^[39], while Pesquera *et al.* showed that strain states in BaTiO₃ membranes laminated on foreign supports were tunable^[50]. Very recently, Degezelle *et al.* reported dynamic strain-driven polarization rotation in freestanding Pb(Zr,Ti)O₃ membranes under mechanical bending^[51]. As an extension of the above-mentioned pioneering work, our freestanding ferroelectric BaTiO₃/BaZrO₃

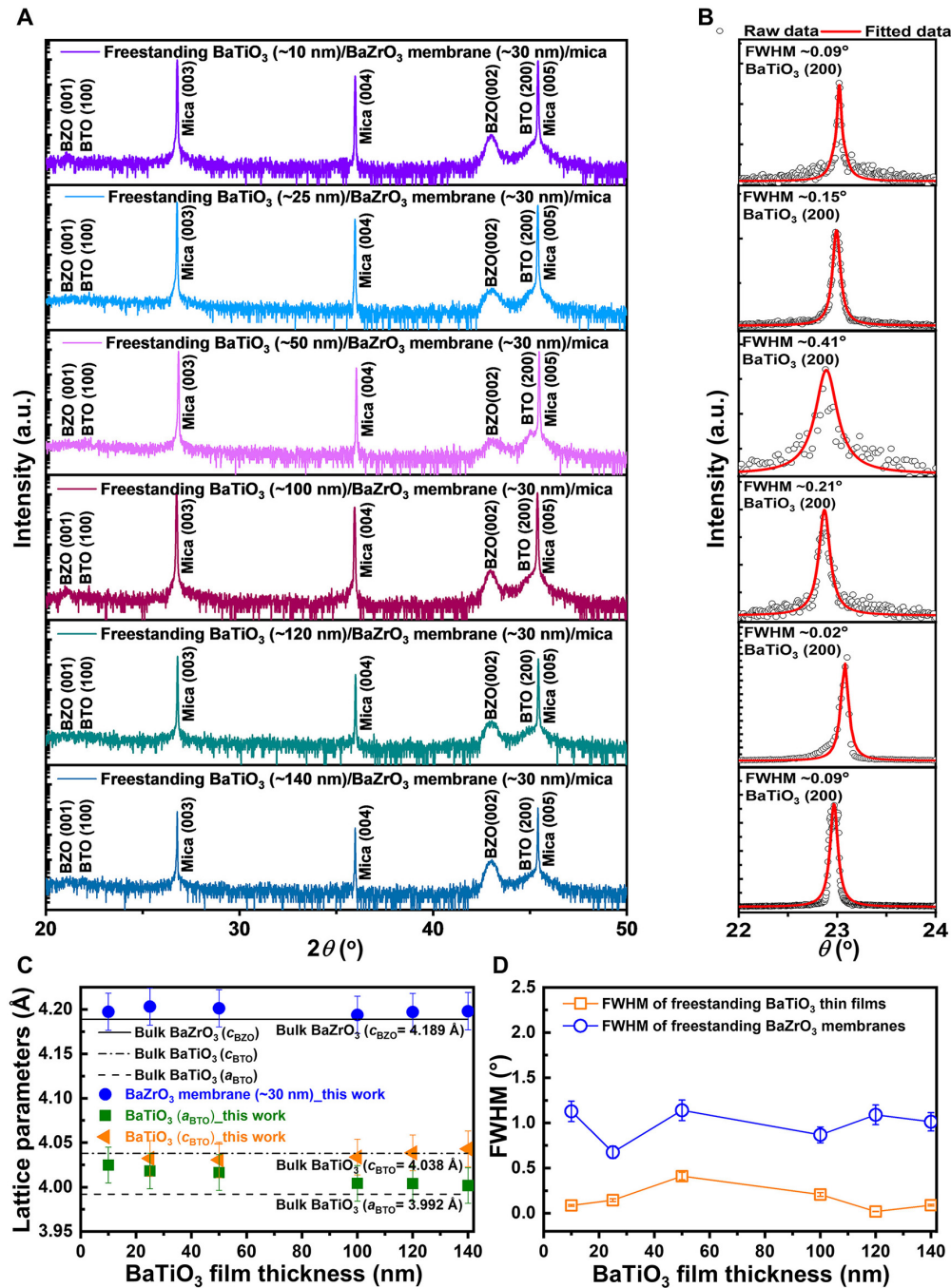


Figure 4. Thickness-dependent XRD analyses of freestanding BaTiO₃/BaZrO₃ membrane heterostructures on mica substrates. (A) The thickness-dependent XRD θ -2 θ results of the as-grown freestanding ferroelectric BaTiO₃/BaZrO₃ membrane heterojunctions. (B) The thickness-dependent rocking-curve measurements of the BaTiO₃ (200) peaks in freestanding BaTiO₃/BaZrO₃ heterojunctions. (C) Thickness-dependent evolution of out-of-plane lattice parameters of the BaTiO₃ and BaZrO₃ layers in BaTiO₃/BaZrO₃ bilayer membranes in comparison with bulk BaTiO₃ and BaZrO₃. (D) A plot of FWHM values of the BaZrO₃ (002) and BaTiO₃ (200) peaks as a function of the BaTiO₃ film thickness. Error bars in (C and D) represent standard errors in the obtained lattice parameters and FWHM values, which are extracted from the Lorentzian fits of the XRD θ -2 θ and rocking-curve results in (A and B), respectively.

membrane heterostructures with high crystallinity would be an excellent candidate of oxide thin-film platforms for reversible strain/flexoelectric engineering of flexible freestanding membrane heterostructures via external mechanical stimuli.

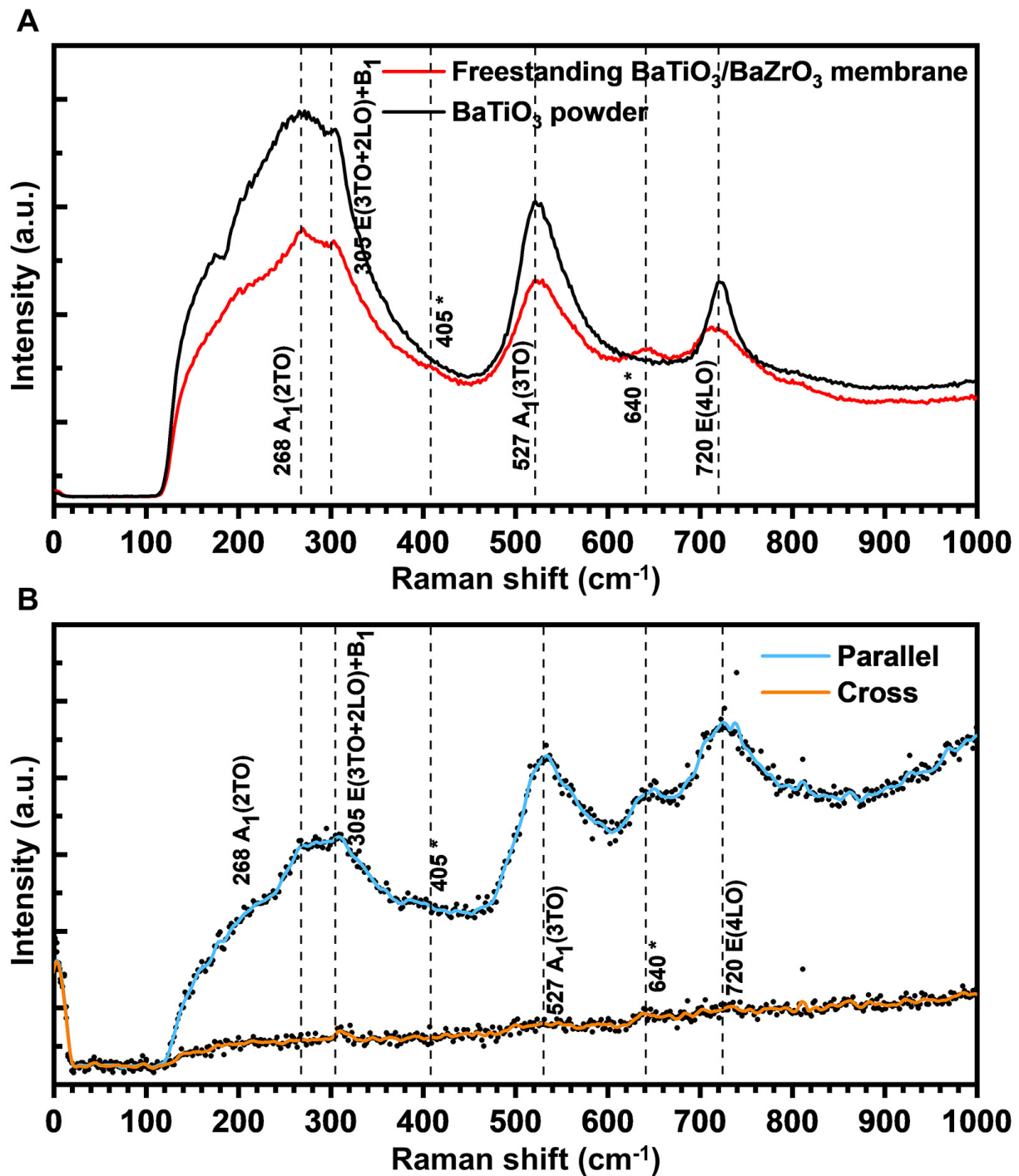


Figure 5. Raman spectra of freestanding ferroelectric BaTiO_3 (~25 nm)/ BaZrO_3 (~30 nm) membrane heterostructures. (A) Raman spectra of the as-integrated freestanding $\text{BaTiO}_3/\text{BaZrO}_3$ membranes heterojunctions. The vertical dashed lines mark principal BaTiO_3 phonons, and a strain-responsive mode appears near ~640 cm^{-1} . (B) Polarization-resolved spectra (parallel versus cross) highlighting selection-rule consistency and the BaTiO_3 overlayer origin of the principal features.

To gain more insight into the ferroelectric properties of the freestanding ferroelectric $\text{BaTiO}_3/\text{BaZrO}_3$ membrane heterostructures, UV-Raman spectroscopy was performed at room temperature. The obtained Raman spectra ($\lambda = 325.0$ nm, 1.5 mW) of our freestanding $\text{BaTiO}_3/\text{BaZrO}_3$ membrane heterojunctions exhibited the characteristic tetragonal BaTiO_3 phonons, including the low-frequency polar $A_1(2\text{TO})/E(3\text{TO})$ modes (~268–305 cm^{-1}) and the higher-frequency $A_1(3\text{TO})$ near ~527 cm^{-1} , together with the high-frequency

$E(4LO)$ branch ($\sim 720\text{ cm}^{-1}$), which was in good agreement with the reference Raman spectra of ferroelectric BaTiO_3 powders (see Figure 5A)^[52–54]. It was further interesting that polarization-resolved Raman measurements [Figure 5B] displayed strong intensity in the parallel geometry and pronounced suppression in cross polarization, consistent with tetragonal selection rules^[53]. Considering that the Raman signals were highly susceptible to microscopic polarization directions and macroscopic domain structures in ferroelectric materials, it was therefore plausible that the as-fabricated freestanding $\text{BaTiO}_3/\text{BaZrO}_3$ heterojunctions were largely in-plane polarized due to biaxial tensile strain imposed by the underlying BaZrO_3 membranes. Nevertheless, direct electrical and atomic-resolution TEM characterizations would provide conclusive evidences of ferroelectric properties and domain structures, respectively. Electrical measurements were previously implemented but extrinsically limited by inevitable structural disorder of the freestanding BaZrO_3 membranes including nano-cracks, warping, and wrinkles, which caused unstable electrical contacts and irreproducible responses. Accordingly, this work mainly focused on establishing feasibility in the sample fabrication, structural integrity, and strain state of freestanding $\text{BaTiO}_3/\text{BaZrO}_3$ heterostructures using comprehensive structural analyses. Herein, Raman spectroscopy appeared as an indirect indicator of crystallographic symmetry and strain-driven polarization states in the as-fabricated $\text{BaTiO}_3/\text{BaZrO}_3$ heterojunctions.

CONCLUSIONS

In summary, we realized a freestanding ferroelectric heterojunctions by epitaxially integrating BaTiO_3 onto single-crystalline BaZrO_3 membranes. We demonstrated that the as-fabricated freestanding ferroelectric $\text{BaTiO}_3/\text{BaZrO}_3$ membrane heterostructures were highly crystalline preserving an epitaxial scheme in conjunction with mechanical flexibility enabled by the removal of rigid substrate clamping. Structural analyses revealed that the underlying BaZrO_3 freestanding membranes served as effective strain-regulating templates, stabilizing in-plane polarized domain configurations in the ferroelectric BaTiO_3 layers while maintaining crystalline integrity. Potentially, our approaches for heterogeneous integration of freestanding oxide membranes via secondary thin-film epitaxy are applicable for rational design of oxide-based flexible microelectronics with strain-controlled ferroelectric domain structures representing enhanced functional properties.

DECLARATIONS

Authors' contributions

Conception and design: Kim, T. H.

Sample fabrication, Sample characterization: Ahmad, M.; Sheeraz, M.; Kim, I. W.; Ahn, C. W.; Kim, T. H.

Raman spectroscopy: Lim, S.; Jang, J. W.; Lee, J. U.

Manuscript writing and revision: Ahmad, M.; Shin, Y. H.; Kim, J.; Kim, T. H.

Manuscript supervision: Shin, Y. H.; Kim, J.; Kim, T. H.

All authors have read and agreed to the published version of the manuscript.

Availability of data and materials

The data that support the findings of this study are available from the corresponding authors upon reasonable request.

AI and AI-assisted tools statement

Not applicable.

Financial support and sponsorship

T.H.K. acknowledges the support of National Research Foundation of Korea (NRF) grants funded by the Ministry of Science and ICT (MSIT) (RS-2025-00554405). This work was also supported by the Korea Institute of Science and Technology (KIST) (26E0181). M.S. acknowledges the support from the Basic Science Research Program through NRF (RS-2023-00249613). J.-U.L acknowledges the Global Learning &

Academic research institution for Master's, PhD students, and postdocs (G-LAMP) Program of the National Research Foundation of Korea (NRF) grant funded by the Ministry of Education (No. RS-2023-00285390) and the Ministry of Science and ICT (MSIT) (RS-2024-00399417). J.K. acknowledges the support from the Ministry of Science and ICT (MSIT) through the National Research Foundation of Korea (NRF): RS-2025-23324084 and RS-2025-25442460. J.K. acknowledges the support from the KAIST institutional program through project Nos. G04240058 and N11250020. Experiments at PLS-II were supported in part by MSIT and POSTECH.

Conflicts of interest

All authors declared that there are no conflicts of interest.

Ethical approval and consent to participate

Not applicable.

Consent for publication

Not applicable.

Copyright

© The Author(s) 2026.

Supplementary Materials

[Supplementary Materials](#)

REFERENCES

1. Fernandez, A.; Acharya, M.; Lee, H. G.; et al. Thin-film ferroelectrics. *Adv. Mater.* **2022**, *34*, 2108841. [DOI](#)
2. Li, T.; Deng, S.; Liu, H.; Chen, J. Insights into strain engineering: from ferroelectrics to related functional materials and beyond. *Chem. Rev.* **2024**, *124*, 7045-105. [DOI](#)
3. Sando, D. Strain and orientation engineering in ABO₃ perovskite oxide thin films. *J. Phys. Condens. Matter.* **2022**, *34*, 153001. [DOI](#) [PubMed](#)
4. Choudhary, N.; Kharat, D.; Kaur, D. Structural, electrical and mechanical properties of magnetron sputtered NiTi/PZT/TiO_x thin film heterostructures. *Surf. Coat. Technol.* **2011**, *205*, 3387-96. [DOI](#)
5. Oh, Y. S.; Wang, L.; Lee, H.; Choi, W. S.; Kim, T. H. Polar perturbations in functional oxide heterostructures. *Adv. Funct. Mater.* **2023**, *33*, 2302261. [DOI](#)
6. Li, Y. L.; Choudhury, S.; Liu, Z. K.; Chen, L. Q. Effect of external mechanical constraints on the phase diagram of epitaxial PbZr_{1-x}Ti_xO₃ thin films - thermodynamic calculations and phase-field simulations. *Appl. Phys. Lett.* **2003**, *83*, 1608-10. [DOI](#)
7. Pan, H.; Zhu, M.; Banyas, E.; et al. Clamping enables enhanced electromechanical responses in antiferroelectric thin films. *Nat. Mater.* **2024**, *23*, 944-50. [DOI](#)
8. Griggio, F.; Jesse, S.; Kumar, A.; et al. Substrate clamping effects on irreversible domain wall dynamics in lead zirconate titanate thin films. *Phys. Rev. Lett.* **2012**, *108*, 157604. [DOI](#)
9. Shi, Q.; Parsonnet, E.; Cheng, X.; et al. The role of lattice dynamics in ferroelectric switching. *Nat. Commun.* **2022**, *13*, 1110. [DOI](#) [PubMed](#) [PMC](#)
10. Ji, H.; Dolbow, J. E. On strategies for enforcing interfacial constraints and evaluating jump conditions with the extended finite element method. *Int. J. Numer. Meth. Eng.* **2004**, *61*, 2508-35. [DOI](#)
11. Moridi, A.; Ruan, H.; Zhang, L.; Liu, M. Residual stresses in thin film systems: Effects of lattice mismatch, thermal mismatch and interface dislocations. *Int. J. Solids Struct.* **2013**, *50*, 3562-9. [DOI](#)
12. Zhang, L.; Yuan, Y.; Lapano, J.; et al. Continuously tuning epitaxial strains by thermal mismatch. *ACS Nano* **2018**, *12*, 1306-12. [DOI](#)
13. Choo, S.; Varshney, S.; Liu, H.; Sharma, S.; James, R. D.; Jalan, B. From oxide epitaxy to freestanding membranes: opportunities and challenges. *Sci. Adv.* **2024**, *10*, eadq8561. [DOI](#) [PubMed](#) [PMC](#)
14. Han, S.; Meng, Y.; Xu, Z.; et al. Freestanding membranes for unique functionality in electronics. *ACS Appl. Electron. Mater.* **2023**, *5*, 690-704. [DOI](#)
15. Haque, M. A.; Saif, M. T. A. Strain gradient effect in nanoscale thin films. *Acta Mater.* **2003**, *51*, 3053-61. [DOI](#)
16. Wang, Q.; Lu, Q.; Zhang, X.; et al. Emergent uniaxial magnetic anisotropy in high-integrity, uniform freestanding LaMnO₃ membranes. *ACS Appl. Mater. Interfaces* **2024**, *16*, 68197-203. [DOI](#) [PubMed](#) [PMC](#)

-
17. Dai, L.; Zhao, J.; Li, J.; et al. Highly heterogeneous epitaxy of flexoelectric BaTiO_{3-δ} membrane on Ge. *Nat. Commun.* **2022**, *13*, 2990. DOI PubMed PMC
 18. Kum, H.; Lee, D.; Kong, W.; et al. Epitaxial growth and layer-transfer techniques for heterogeneous integration of materials for electronic and photonic devices. *Nat. Electron.* **2019**, *2*, 439–50. DOI
 19. Huang, Z.; Ariando; Wang, X. R.; et al. Interface engineering and emergent phenomena in oxide heterostructures. *Adv. Mater.* **2018**, *30*, 1802439. DOI
 20. Lee, Y.; Choi, S. H.; Kim, H.; Yoo, J. Epitaxy of emerging materials and advanced heterostructures for microelectronics and quantum sciences. *Small Methods* **2025**, *9*, 2401815. DOI PubMed PMC
 21. Salles, P.; Caño, I.; Guzman, R.; et al. Facile chemical route to prepare water soluble epitaxial Sr₃Al₂O₆ sacrificial layers for free-standing oxides. *Adv. Mater. Interfaces* **2021**, *8*, 2001643. DOI
 22. Pesquera, D.; Fernández, A.; Khestanova, E.; Martin, L. W. Freestanding complex-oxide membranes. *J. Phys. Condens. Matter* **2022**, *34*, 383001. DOI PubMed
 23. Sheeraz, M.; Jung, M. H.; Kim, Y. K.; et al. Freestanding oxide membranes for epitaxial ferroelectric heterojunctions. *ACS Nano* **2023**, *17*, 13510–21. DOI
 24. Nian, L.; Sun, H.; Wang, Z.; et al. Sr₄Al₂O₇: a new sacrificial layer with high water dissolution rate for the synthesis of freestanding oxide membranes. *Adv. Mater.* **2024**, *36*, e2307682. DOI
 25. Bakaul, S. R.; Serrao, C. R.; Lee, M.; et al. Single crystal functional oxides on silicon. *Nat. Commun.* **2016**, *7*, 10547. DOI PubMed PMC
 26. Chang, Y. W.; Wu, P. C.; Yi, J. B.; et al. A fast route towards freestanding single-crystalline oxide thin films by using YBa₂Cu₃O_{7- δ} as a sacrificial layer. *Nanoscale Res. Lett.* **2020**, *15*, 172. DOI PubMed PMC
 27. Takahashi, R.; Lippmaa, M. Sacrificial water-soluble BaO layer for fabricating free-standing piezoelectric membranes. *ACS Appl. Mater. Interfaces* **2020**, *12*, 25042–9. DOI PubMed
 28. Peng, H.; Lu, N.; Yang, S.; et al. A Generic sacrificial layer for wide-range freestanding oxides with modulated magnetic anisotropy. *Adv. Funct. Mater.* **2022**, *32*, 2111907. DOI
 29. Kim, H.; Chang, C. S.; Lee, S.; et al. Remote epitaxy. *Nat. Rev. Methods Primers* **2022**, *2*, 40. DOI
 30. Park, B. I.; Kim, J.; Lu, K.; et al. Remote epitaxy: fundamentals, challenges, and opportunities. *Nano Lett.* **2024**, *24*, 2939–52. DOI
 31. Lee, J. H.; Duong, N. X.; Jung, M. H.; et al. Reversibly controlled ternary polar states and ferroelectric bias promoted by boosting square-tensile-strain. *Adv. Mater.* **2022**, *34*, e2205825. DOI
 32. Choi, K. J.; Biegalski, M.; Li, Y. L.; et al. Enhancement of ferroelectricity in strained BaTiO₃ thin films. *Science* **2004**, *306*, 1005–9. DOI
 33. Wang, X.; Deng, X.; Wen, H.; Li, L. Phase transition and high dielectric constant of bulk dense nanograin barium titanate ceramics. *Appl. Phys. Lett.* **2006**, *89*, 162902. DOI
 34. Panomsuwan, G.; Manuspiya, H. A comparative study of dielectric and ferroelectric properties of sol-gel-derived BaTiO₃ bulk ceramics with fine and coarse grains. *Appl. Phys. A* **2018**, *124*, 713. DOI
 35. Lin, E. L.; Posadas, A. B.; Zheng, L.; et al. Atomic layer deposition of epitaxial ferroelectric barium titanate on Si (001) for electronic and photonic applications. *J. Appl. Phys.* **2019**, *126*, 064101. DOI
 36. Fortunato, E.; Barquinha, P.; Martins, R. Oxide semiconductor thin-film transistors: a review of recent advances. *Adv. Mater.* **2012**, *24*, 2945–86. DOI PubMed
 37. He, F.; Wells, B. O. Lattice strain in epitaxial BaTiO₃ thin films. *Appl. Phys. Lett.* **2006**, *88*, 152908. DOI
 38. Damodaran, A. R.; Breckenfeld, E.; Chen, Z.; Lee, S.; Martin, L. W. Enhancement of ferroelectric Curie temperature in BaTiO₃ films via strain-induced defect dipole alignment. *Adv. Mater.* **2014**, *26*, 6341–7. DOI PubMed
 39. Elangovan, H.; Barzilay, M.; Seremi, S.; et al. Giant superelastic piezoelectricity in flexible ferroelectric BaTiO₃ membranes. *ACS Nano* **2020**, *14*, 5053–60. DOI
 40. Dong, G.; Li, S.; Yao, M.; et al. Super-elastic ferroelectric single-crystal membrane with continuous electric dipole rotation. *Science* **2019**, *366*, 475–9. DOI
 41. Azar, S. A.; Al-zoubi, I.; Mousa, A. A.; Masharfe, R. S.; Jaradat, E. K. Investigation of electronic, optical and thermoelectric properties of perovskite BaTMO₃ (TM = Zr, Hf): First principles calculations. *J. Alloys Compd.* **2021**, *887*, 161361. DOI
 42. Vera, C. Y. R.; Ding, H.; Peterson, D.; et al. A mini-review on proton conduction of BaZrO₃-based perovskite electrolytes. *J. Phys. Energy* **2021**, *3*, 032019. DOI
 43. Kolodiaznyy, T.; Pulphol, P.; Vittayakorn, W.; Vittayakorn, N. Giant suppression of dielectric loss in BaZrO₃. *J. Eur. Ceram. Soc.* **2019**, *39*, 4144–8. DOI
 44. Harbola, V.; Xu, R.; Hong, S. S. Experimental progress in freestanding oxide membranes designed by epitaxy. *Adv. Phys. X.* **2025**, *10*, 2450538. DOI

45. Duong, N. X.; Bae, J.; Jeon, J.; et al. Polymorphic phase transition in BaTiO₃ by Ni doping. *Ceram. Int.* **2019**, *45*, 16305-10. [DOI](#)
46. Xu, C.; Liang, W.; Hong, P.; Hu, Y.; Yang, Z.; Pang, H. Lignin/graphene oxide composite coating loaded with zinc ions and its photothermal conversion and self-healing anticorrosion properties. *Microstructures* **2025**, *5*, 2025037. [DOI](#)
47. Xu, R.; Huang, J.; Barnard, E. S.; et al. Strain-induced room-temperature ferroelectricity in SrTiO₃ membranes. *Nat. Commun.* **2020**, *11*, 3141. [DOI](#) [PubMed](#) [PMC](#)
48. Huang, S.; Xu, S.; Ma, C.; et al. Ferroelectric order evolution in freestanding PbTiO₃ films monitored by optical second harmonic generation. *Adv. Sci.* **2024**, *11*, e2307571. [DOI](#) [PubMed](#) [PMC](#)
49. Zhou, M.; Peng, K.; Tan, Y.; Yang, T.; Chen, L.; Nan, C. Domain evolution, dielectric and piezoelectric response in bent freestanding PbTiO₃ ferroelectric nanowires. *Acta Mater.* **2025**, *288*, 120805. [DOI](#)
50. Pesquera, D.; Parsonnet, E.; Qualls, A.; et al. Beyond substrates: strain engineering of ferroelectric membranes. *Adv. Mater.* **2020**, *32*, e2003780. [DOI](#)
51. Degezelle, A.; Burcea, R.; Gemeiner, P.; et al. Strain-induced polarization rotation in freestanding ferroelectric oxide membranes. *Adv Electron Mater* **2025**, *11*, e00266. [DOI](#)
52. Didomenico, M.; Wemple, S. H.; Porto, S. P. S.; Bauman, R. P. Raman spectrum of single-domain BaTiO₃. *Phys Rev* **1968**, *174*, 522-30. [DOI](#)
53. Marssi, M. E.; Marrec, F. L.; Lukyanchuk, I. A.; Karkut, M. G. Ferroelectric transition in an epitaxial barium titanate thin film: Raman spectroscopy and x-ray diffraction study. *J. Appl. Phys.* **2003**, *94*, 3307-12. [DOI](#)
54. Silva, J. P. B.; Sekhar, K. C.; Almeida, A.; Moreira, J. A.; Pereira, M.; Gomes, M. J. M. Influence of laser repetition rate on ferroelectric properties of pulsed laser deposited BaTiO₃ films on platinized silicon substrate. *Appl. Phys. A* **2013**, *113*, 379-84. [DOI](#)

Disclaimer/Publisher's Note: All statements, opinions, and data contained in this publication are solely those of the individual author(s) and contributor(s) and do not necessarily reflect those of OAE and/or the editor(s). OAE and/or the editor(s) disclaim any responsibility for harm to persons or property resulting from the use of any ideas, methods, instructions, or products mentioned in the content.



© The Author(s) 2026. Open Access This article is licensed under a Creative Commons Attribution 4.0 International License (<https://creativecommons.org/licenses/by/4.0/>), which permits unrestricted use, sharing, adaptation, distribution and reproduction in any medium or format, for any purpose, even commercially, as long as you give appropriate credit to the original author(s) and the source, provide a link to the Creative Commons license, and indicate if changes were made.